Earthquakes and Structures, *Vol. 15, No. 5 (2018) 555-564*
DOI: https://doi.org/10.12989/eas.2018.15.5.555

Response of structure with controlled uplift using footing weight

X. Qin* and N. Chouw

Department of Civil and Environmental Engineering. The University of Auckland, Auckland Mail Centre, Private Bag 92019, Auckland 1142, New Zealand

(Received June 10, 2018, Revised August 14, 2018, Accepted September 13, 2018)

Abstract. Allowing structures to uplift in earthquakes can significantly reduce or even avoid the development of plastic hinges within the structure. The permanent deformations in the structure can thus be minimized. However, uplift of footings can cause additional horizontal movements of a structure. With an increase in movement relative to adjacent structures, the probability of pounding between structures increases. This experimental study reveals that the footing mass can be used to control the vertical displacement of footing and thus reduce the horizontal displacements of an upliftable structure. A four storey model structure with plastic hinges and uplift capability was considered. Shake table tests using ten different earthquake records were conducted. Three different footing masses were considered. It is found that the amplitude of footing uplift can be greatly reduced by increasing the mass of the footing. As a result, allowing structural uplift does not necessary increase the horizontal displacement of the structure. The results show that with increasing footing weight, the interaction between structural and footing response can increase the contribution of the higher modes to the structural response. Consequently, the induced vibrations on secondary structure increase.

Keywords: structural uplift; scaling; dimensional analysis; low-damage seismic design; induced vibration

1. Introduction

Current seismic design of structures has been strongly shaped by capacity design where damage to structures is permitted and life safety ensured. However, observations of damage to infrastructure from past major earthquakes (e.g., Chouw and Hao 2012) indicate that this approach often results in damage that either leads to significant economic losses due to long downtime, or damage that is irreparable due to the high cost involved. Also, the plastic hinge development during aftershocks can accumulate damage in structures (Qin *et al*. 2018). Hence, in recent years the philosophy of ‘damage avoidance’ is recommended in seismic design. Various methods to implement this philosophy are currently under investigation. One way to minimize plastic deformation in a structure is to allow the structure to uplift, i.e., part of the footing can temporary separate from the supporting ground, whenever the overturning moment exceeds the restraining moment provided by the self-weight (Kafle *et al*. 2015).

Structural uplift has been considered as a possible earthquake-proof solution for structures since 1960, after the Valdivia earthquake in Chile (Housner 1963). It was reported that a number of tall, slender structures survived the earthquake, while other more stable appearing structures were severely damaged. Following this observation, a number of studies have proven that uplift can be beneficial to the seismic response of a structure (Ichinose 1986, Psycharis 1991, Chopra and Yim 1985, Fardis *et al*. 2013). Ichinose (1986) studied the response of flexible structures with uplift using a finite-element approach. It was concluded that the flexural deformation of the structure decreases when uplift amplitude increases. Analytical formulations to calculate the response of a structure with uplift have also been developed (Psycharis 1991, Chopra and Yim 1985). Psycharis (1991) used analytical results to establish a set of equations that calculates the reduction of structural deformation due to uplift. Chopra and Yim (1985) considered dynamic force equilibrium to derive a set of equations of motion to determine the response of structures with uplift. They proposed a formula to estimate the maximum deformation and base shear in an upliftable structure.

In recent years, allowing wall members of the structure to uplift was also found to be beneficial to the seismic resistance of structures (Fardis *et al*. 2013, Loo *et al*. 2012). A few structures have been built with uplift capability, e.g., the Rangitikei Railway Bridge (Beck and Skinner 1973, Chen *et al*. 2006) and a 30 m tall industrial chimney (Sharpe and Skinner 1983) in New Zealand. In the retrofit programme of the Lions Gate Bridge in Vancouver (Dowdell and Hamersley 2000), structural uplift was also implemented. A number of design guidelines for structures with uplift have been proposed (e.g., FEMA 2000, Kelly 2009). Most studies on structural uplift focused on the reduction of structural deformations. Not much attention has been paid to the contribution of uplift induced rigid body motion to the structural response. Uplift of footings can, in fact, increase the horizontal movement of a structure. Consequently, adjacent structures can have a high pounding potential.

*Corresponding author, Ph.D.
E-mail: xqin009@aucklanduni.ac.nz

ISSN: 2092-7614 (Print), 2092-7622 (Online)

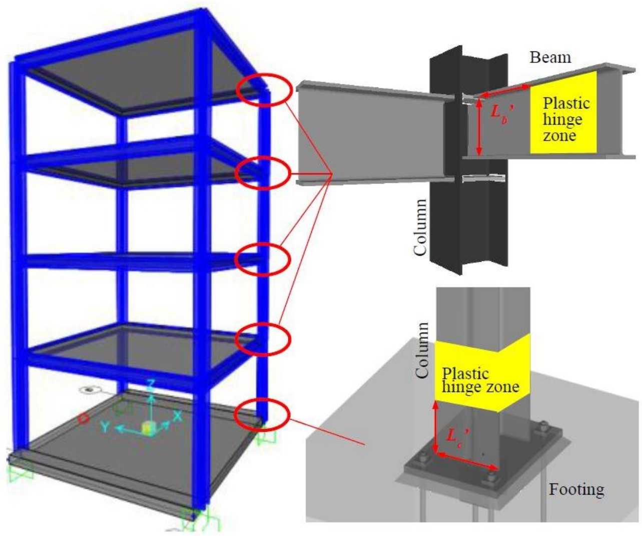

Fig. 1 Locations of plastic hinge zone in the prototype with an assumed fixed base

This work experimentally investigated whether the footing response of upliftable structures can be reduced by the weight of the footing. A model of a multi-storey upliftable structure with possible plastic hinge development was considered. The seismic response of the structure with a fixed base or allowable uplift with different footing weights was obtained using shake table testing. Based on the response of the structure, the induced vibrations in the structure were also studied.

2. Modelling and experiment

2.1 Prototype structure

The prototype structure is a four storey building designed according to the New Zealand Design Standard. Fig. 1 shows the layout of the building. The inter-storey height of the building is 3.15 m and the width of the structure is 7 m. The column and beam sections of the structure are 310UC158 and 410UB53.7, respectively. The beam and column stiffness ratio is 1 to 8. The seismic mass of the structure is 29 t and 24 t for the floor and roof levels, respectively.

Plastic hinge development is tolerated in the building, with a ductility demand of 1.5. Plastic hinge can take place in the zone close to the end of the beams and base of the columns as indicated in Fig. 1. The location of the plastic hinge zone in the beam as defined by NZS1170.5 (NZS, 2004a) is L_b' away from the beam to column connection (Fig. 1), where L_b' is the depth of the beam (403 mm). The plastic hinge zone in the column is 327 mm away from the column footing connection. This distance is determined according to the depth of the column (L_c').

2.2 Similitude and model scaling

The prototype is scaled for shake table experiments. The scale factors are calculated from dimensionless parameters

Table 1 Scale factors

Parameter	Prototype	Scale factor	Model
Storey height (*h*)	3.15 m	S_L=15	0.21 m
Footing width (2*b*)	7 m	S_L=15	0.47 m
Mass of each floor (*m*)	29 t	S_m=1200	24.2 kg
Mass of roof (*m*)	24 t	S_m=1200	20 kg
Mass of footing (*m*)	29 t	S_m=1200	24.2 kg
Plastic hinge zone (L_b')	403 mm	S_L=15	26.8 mm
Plastic hinge zone (L_c')	327 mm	S_L=15	21.8 mm
Lateral stiffness (*k*)	62,100 kN/m	S_k=1200	51.75 kN/m
Ground acceleration (*a*)	PGA	S_a=15	PGA/15
Fundamental frequency (ω)	1.56 Hz	S_ω=1	1.56 Hz

(π) obtained from Buckingham π theorem and dimensional analysis (Buckingham 1914). The dimensionless parameters consist of six physical quantities. These quantities include the geometry (*l*), mass (*m*), stiffness (*k*) and elastic deformation (*u*) of the structure, the duration (T_e) and horizontal acceleration (*a*) of the excitation.

Among the six quantities, three physical dimensions are deduced, i.e., mass (*M*), time (*T*) and length (*L*). Buckingham (1914) has demonstrated that for a system with eight quantities and three physical dimensions, the response of the structure with uplift can be characterized by three non-dimensionalised parameters (π)

$$\pi_1 = \frac{ku}{ma} \tag{1}$$

$$\pi_2 = T_e\sqrt{\frac{a}{l}} \tag{2}$$

$$\pi_3 = T_e\sqrt{\frac{k}{m}} \tag{3}$$

The parameter π_1 is the ratio of elastic restoring force to inertia force, which is identical to Cauchy's number. π_2 describes the relationship between the predominant frequency and amplitude of the excitation and the geometrical dimension of the structure. π_3 is the ratio of the predominant frequency of excitations to the structural natural frequency.

Table 1 shows the scale factors. In the conventional scaling approach for shake table experiments, the scale factors for dimension and mass of the prototype are predefined. The response of structures with uplift or plastic hinge development is nonlinear. Thus the frequency of the system cannot be scaled (i.e., S_ω=1).

The scale factor for dimensions (S_L) and the mass (S_m) of the prototype are predefined to be 15 and 1200, respectively. The scale factor of the ground acceleration amplitude (S_a) is calculated to be 15. Table 1 summarizes the scale factors. Nine relevant parameters are scaled accordingly.

2.3 Structural model

The dimensions of the model structure are shown in

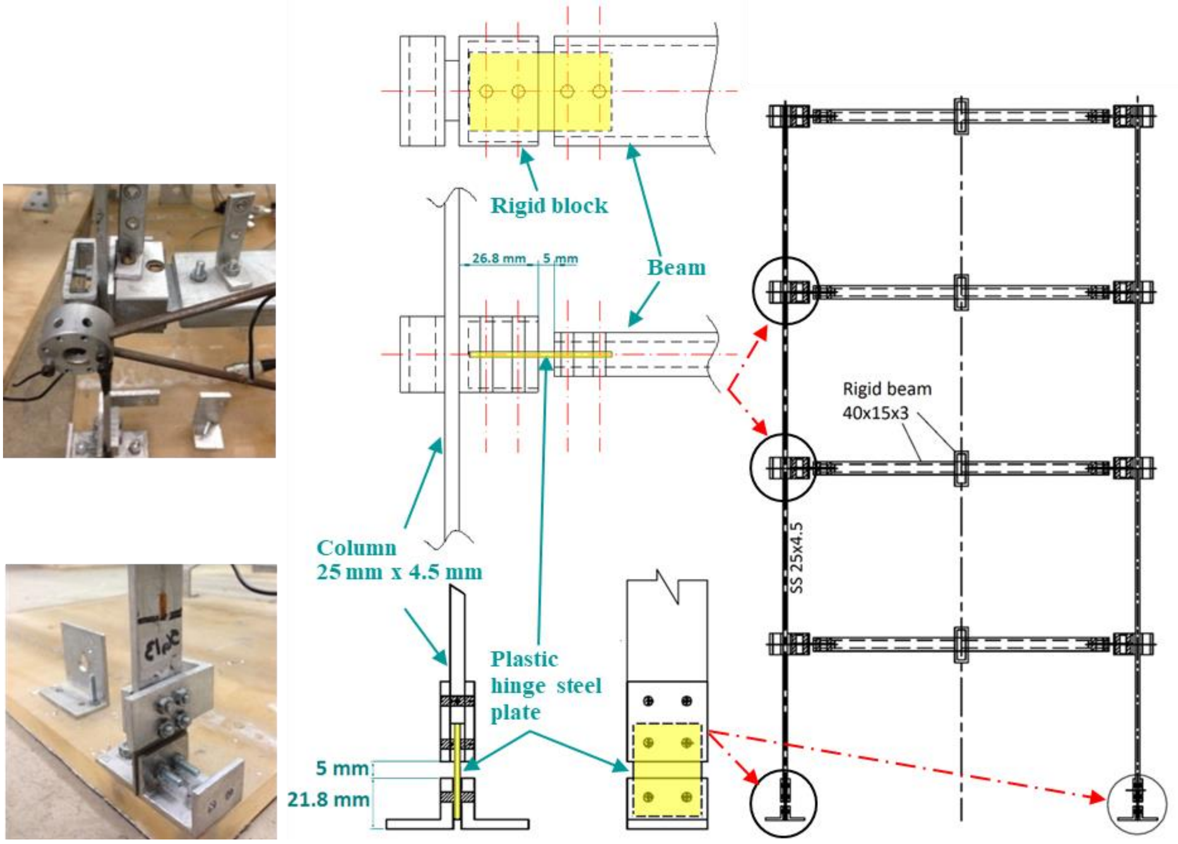

Fig. 2 Plastic hinge in the structure

Table 1. The total masses at each floor and roof of the structure were 24.2 kg and 20.4 kg, respectively. The storey height and the total height of the structure were 210 mm and 840 mm, respectively. The foundation was constructed from a 470 mm×470 mm×22 mm rigid plates. The columns were constructed using aluminium sections of cross section 4.5 mm×25 mm.

The plastic hinge zones in the structure are defined according to those in the prototype. Fig. 2 shows the details of the beam to column connection. To allow the plastic hinge development in the beams, a thin steel plate was bolted in between the beam and the rigid block on the column (see top sketch in Fig. 2). The open length of the steel plate was 5 mm. This open length was the location where the plastic hinge was designed to develop in the beam during an earthquake. The length of the rigid block was 26.8 mm (see Fig. 2). This length ensured the plastic hinge zone in the beam was located L_b' away from the beam-to-column connection (see Table 1).

The plastic hinges in the columns are only tolerated at the lower ends of the columns on the ground floor (above column-to-footing connection). Fig. 2 shows the details of the column-to-footing connection. A thin steel plate was bolted into the column and two rigid L plates on the footing. The L sections were considered to be rigid and had a height of 21.8 mm. This height ensured that the plastic deformation of the column only took place at the zone.

Two different thicknesses (2 mm and 1.6 mm) of steel plate were used for the case of an elastic structure and a structure with possible plastic hinge development, respectively. The width of the steel plate was determined using a computer model. In the elastic condition, the mode shapes and the corresponding frequencies of the structure matched those of the prototype. The widths were 19 mm and 24 mm for the 2 mm and 1.6 mm plate, respectively. When plastic hinge develops, the steel plates used for the plastic hinge were replaced after each experiment to ensure that the structure had the same initial condition.

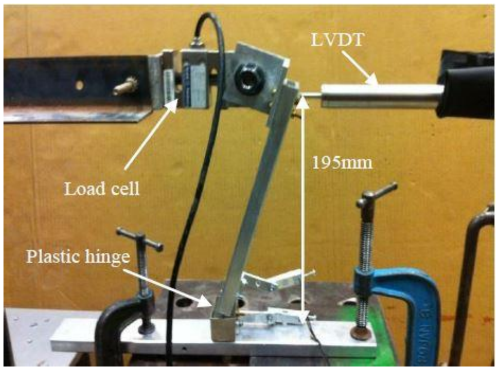

Fig. 3 Test on the plastic hinge

2.4 Plastic hinge development

A cyclic test was performed on a beam with the 1.6 mm steel plate installed to determine the moment capacity of the plastic hinge. Fig. 3 shows the experimental setup. A total of 15 cyclic displacements were applied. The amplitudes were increased for each of the three cycles. A total of five

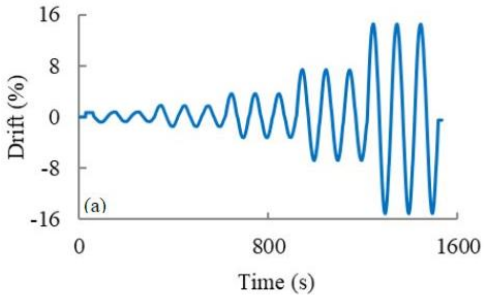

(a)

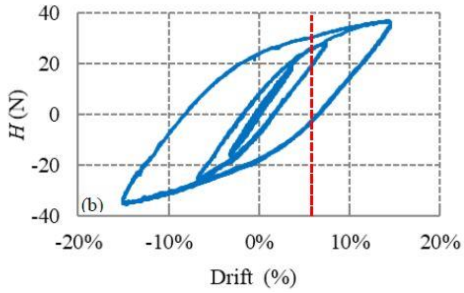

(b)

Fig. 4 Cyclic test: (a) applied displacement and (b) behaviour of the plastic hinge

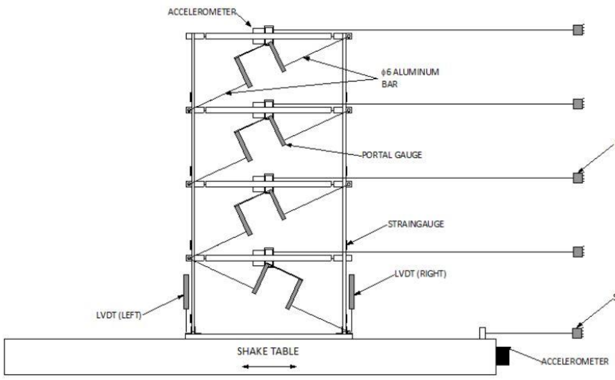

Fig. 5 Experimental setup of the structure

amplitudes were considered in total. These amplitudes were equivalent to 1%, 2%, 4%, 8% and 16% inter-storey drift. The time history of the applied cyclic drift is shown in Fig. 4(a). Load cells were used to measure the shear force applied (*H*). Fig. 4(b) shows the force-drift relationship of the plastic hinge. It was found that the connection started to yield at 4.9% drift (see dashed vertical line in Fig. 4(b)).

Draw-wire actuators were located at each level of the structure to measure the horizontal displacement relative to the ground. Portal gauges were attached to diagonal bracings at each storey, to measure the inter-storey displacement. Strain gauges were attached to each column base to record strain for calculating bending moments. The acceleration at each floor level of the structure was also measured (Fig. 5). By using a free vibration test, the fundamental period of the structure was found to be T_n=0.64 s with a damping ratio ξ=13%. The relatively high value of damping ratio was attributed mainly to the friction of the instrumentation such as the portal gauges and the draw-wire actuators.

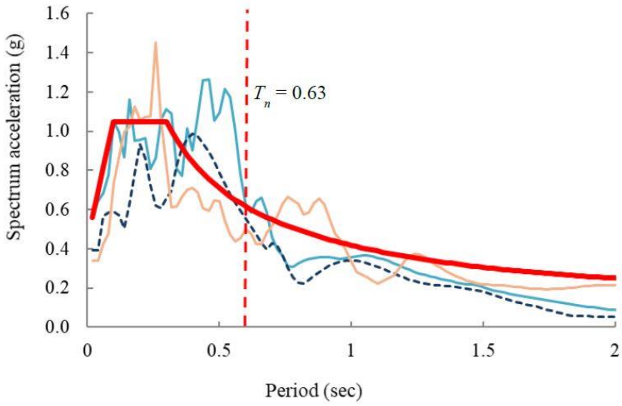

Fig. 6 Fitting selected earthquake to the target spectrum

Table 2 Summary of ground motion characteristics

Record	Earthquake	Station	Mw	*D* (km)	PGA (g)	Forward directivity
1	San Fernando	Pacoima Dam	6.6	1.81	0.58	Y
2	Northridge	Pacoima Dam (downstr)	6.7	7.01	0.41	Y
3	Tabas	Tabas	7.4	2.10	0.35	Y

2.5 Ground excitations

The excitations used in the experiments were earthquake records, scaled according to a target spectrum obtained from NZS 1170.5 (2004a). The target spectrum was specified for the Palmerston North region, that is located in the southern part of the North Island of New Zealand. This region is where the main faults of the North Island are concentrated. To define the target spectrum of this region, the classification of the site was assumed to be soil type A (strong rock). The hazard factor (*Z* value) of the site is 0.45. The return period of the events is considered to be 500 years. The prototype has a design life of 50 years and an annual probability of exceedance of 10%. Fig. 6 shows the spectrum accelerations of the records selected and the design spectrum. The response spectra were calculated using a damping ratio of 5%.

According to NZS1170.5 (2004a), the selected records should be representative of the source-to-site distances and fault mechanisms of the earthquake events that contribute to the target design spectra of the site, over the period range of interest (NZS 1170.5). Oyarzo-Vera *et al.* (2012) investigated the seismological signature of different zones in the North Island of New Zealand. For Palmerston North, the zone corresponds to the near-fault region, which contains the most active strike-slip faults as well as numerous reverse and normal faults. It was recommended that the selected ground motions are recorded with a shortest distance of up to 10 km from the rupture surface (*D*). Three earthquake records were selected based on these criteria. The ground motions were obtained from the PEER NGA strong motion data base (PEER) and are summarized in Table 2. The selected records were scaled according to the target spectrum. The vertical dashed line in Fig. 6 represents the fundamental period (T_n) of the prototype structure with a fixed-base assumption.

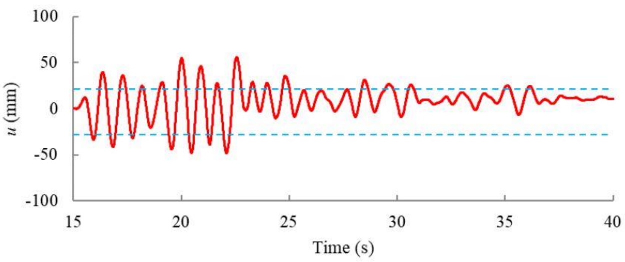

Fig. 7 Effect of plastic deformation on top displacement due to R3

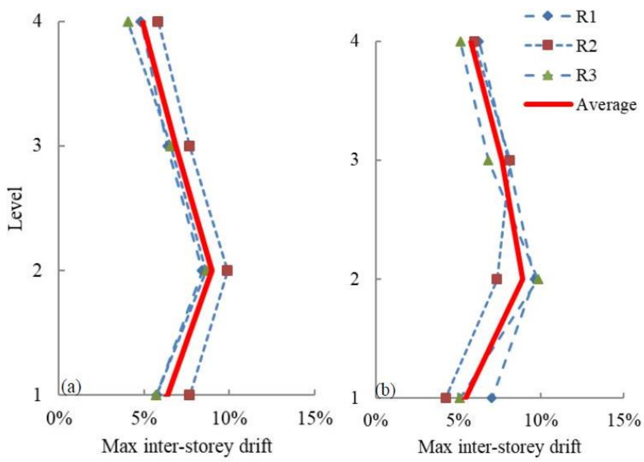

(a) (b)

Fig. 8 Inter-storey drift (a) with and (b) without plastic hinge

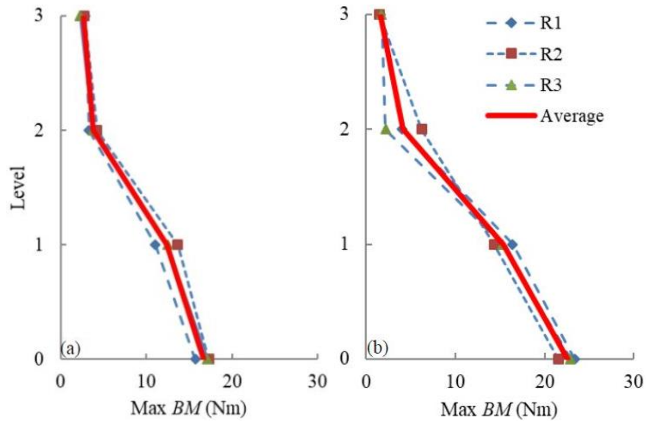

(a) (b)

Fig. 9 Bending moment distribution (a) with and (b) without plastic hinge development

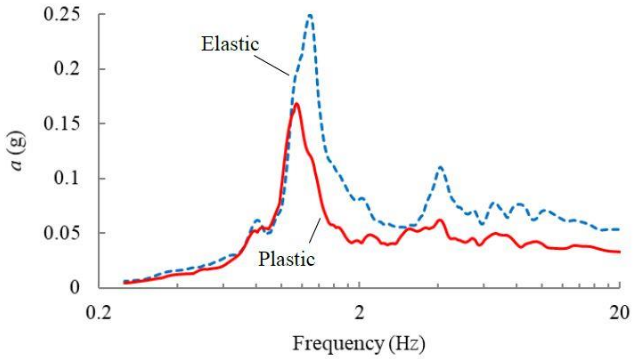

Fig. 10 Reduction of spectrum acceleration at the roof level as a result of plastic hinge development due to R3

3. Performance of the structure

3.1 Response of structure with plastic hinge

Fig. 7 shows the time history of the horizontal displacement (u) at the top of the structure when subjected to earthquake R3. When plastic hinge is permitted, the structure exceeds on 14 occasions the elastic limit (horizontal dashed line in Fig. 7) resulting in a permanent lateral displacement of 12.7 mm.

Fig. 8 summarizes the maximum inter-storey drifts due to different excitations. While Fig. 8(a) illustrates the case of an elastic structure (using 2 mm plate), Fig. 8(b) represents the case considering plastic hinge development (using 1.6 mm plate). As shown, plastic hinge development in the structure caused a larger maximum drifts at the first and second floors. In contract, the drifts at the third and top floors of the structure decreased. On average, the maximum inter-storey drifts from the first to the top floors of the structure were 5.6%, 7.6%, 6.2% and 4.6%, respectively. Without plastic hinge development, the corresponding maximum inter-storey drifts were 5.3%, 7.3%, 6.8% and 4.9%.

Fig. 9 compares the maximum bending moment at different storeys. The values were calculated by summing the bending moments at the lower end of the four columns of each storey. Because of the plastic hinge development at the first and second floors, the storey bending moments at these two floors were reduced significantly. Without plastic hinge development, the average maximum storey bending moments at the first and second floors were 20.1 Nm and 12.7 Nm, respectively. When plastic hinges developed, the corresponding maximum bending moments were only 14.4 Nm and 11.3 Nm. The storey bending moments at the top two floors of the structure were similar, with and without plastic hinge development.

Induced vibrations are of concern to secondary structures. In order to reveal the effect of plastic hinge development on induced vibrations, response spectra of the horizontal accelerations at the top of the structure are calculated (Fig. 10). A damping ratio of 5% is assumed. The spectrum values represent the estimated maximum responses of secondary structures attached to the roof level. It is found that plastic hinge development can reduce the impact of vibration on the secondary structure induced from primary structure. For frequencies lower than 1.1 Hz, the spectrum values for the structure with and without plastic hinge development are similar. For the structure with plastic hinges, in the frequencies range greater than 1.1 Hz, the spectrum values are always smaller than those of the elastic structure. Since secondary structures generally have high frequencies, reducing the spectrum acceleration at the regions of high frequencies will reduce the response of secondary structures.

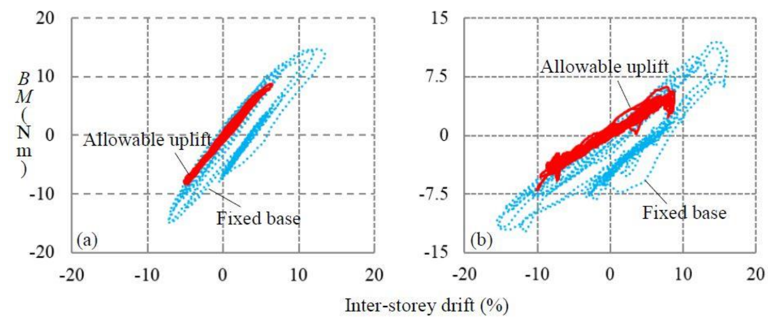

Fig. 11 Effect of uplift on plastic hinge development and bending moment of (a) ground and (b) first floors of the structure due to R3

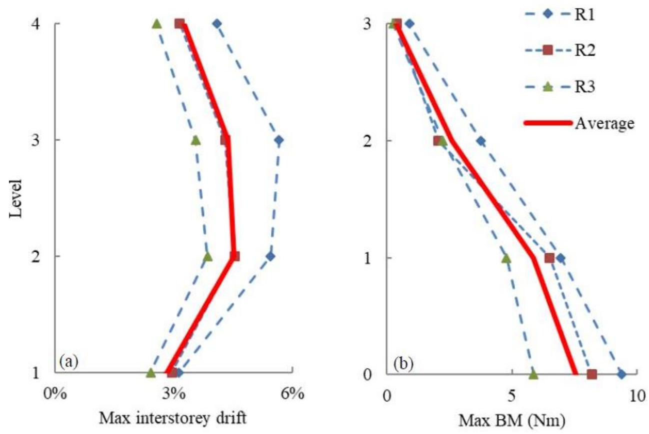

Fig. 12 Maximum (a) inter-storey drift and (b) storey bending moment at each floor of the structure with uplift and allowable plastic hinge (w_f/w_t=27%)

3.2 Effect of uplift on the structure

A series of shake table tests were conducted on the structure with allowable uplift. For all experiments considering footing uplift, plastic hinge development in the structure was permitted, i.e., 1.6 mm thick plates were used at the plastic hinge zones. Fig. 11 compares the moment-drift relationship in the first two floors of the structure. With a fixed base, the plastic hinge developments were evidenced at the first two floors. However, when uplift was permitted, the structure remained elastic, i.e., no plastic hinge development was found. In all cases of three excitations considered, no residual drift was evidenced in the structure when uplift was permitted.

Fig. 12 shows the maximum inter-storey drift and storey bending moment at each level of the structure with uplift. Compared to the drift of the nonlinear structure with an assumed fixed base (Fig. 8(a)), the inter-storey drift at each floor level of the structure became smaller because of uplift. On average, the maximum inter-storey drift from the first to the top level of the structure was 3%, 5%, 4% and 3%, respectively.

The storey bending moment at each floor of thestructure was also smaller as a consequence of uplift of the structure. On average, the maximum storey bending moment in the structure from the ground to the roof was 7.08 Nm, 5.85 Nm, 2.59 Nm and 0.38 Nm, respectively. Compared to the structure with a fixed base and plastic hinge development, the corresponding storey bending moment was 54.9%, 48.2%, 23.8% and 82.7% smaller (see also Fig. 9(a)).

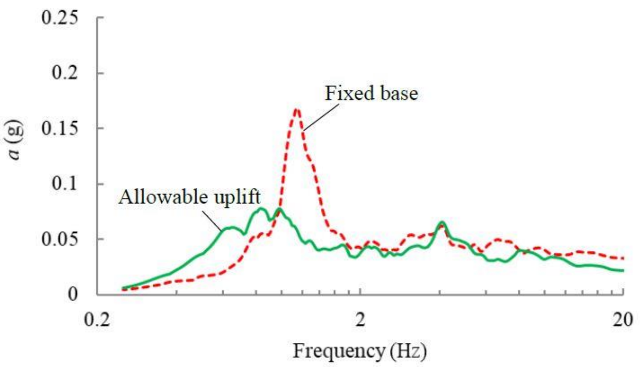

Fig. 13 Spectrum acceleration at the top of the nonlinear structure with uplift due to R3

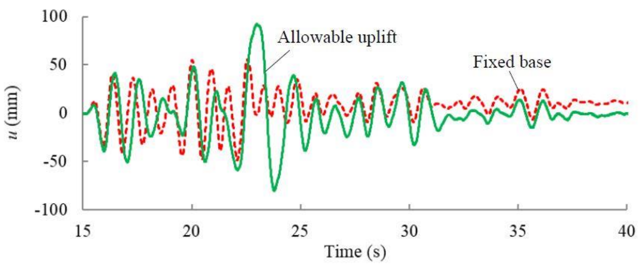

Fig. 14 Consequence of uplift for the top horizontal displacement due to R3

Fig. 13 shows the response spectra of acceleration at the roof level of the nonlinear structure with and without allowable uplift. The spectra are calculated with 5% damping ratio. As shown, the structure with uplift causes a larger induced vibration on the secondary structure in the frequency region below 1.05 Hz. In the frequency range between 1.05 Hz to 1.97 Hz, there is a great reduction in of induced vibrations on the secondary structure. This is because when uplift was initiated, the deformation of the structure reduced, thus the induced vibration associated with the structural vibration due to the deformation of the strucutre (in the freqnecy range between 1.05 Hz to 1.97 Hz) was also redced. On the other hand, the rocking response induced and additional response with a lower frequency than the fundamental frequency of the sttrucutre (i.e., lower than 1.05 Hz).Overall, in the higher frequencies

Table 3 Change of footing mass

	Original	With additional
Footing weight w_f (N)	15.7	89.3
M_R (Nm)	18.2	36.5
Total storey weight w_t (N)	57.8	57.8
w_t/w_f	27%	154%

region (greater than 1.97 Hz) the spectrum accelerations in the structure with uplift are smaller than those in the structure with a fixed base. This observation is also evidenced in the case of other excitations. Secondary structures are generally of relatively higher frequency, thus structural uplift is more effective in reducing the effect of induced vibrations on the secondary structure compared to the influence of allowing plastic hinge development (see Fig. 10).

Because of the footing rotation, the horizontal displacement of the structure relative to ground, increased. Fig. 14 compares the horizontal displacement at the roof of the structure with and without uplift. In the case of a fixed base, the maximum top horizontal displacement was 55.6 mm. In comparison, allowing the structure to uplift caused much larger displacement of 92.4 mm, i.e., a 66.2% increase. The large increase in horizontal displacement will increase the relative movement between adjacent structures and may lead to pounding damage.

Compared to the fixed-base structure the vibration period of the structure with uplift is longer (Fig. 14). This explains why the vibrations induced into the secondary structures, from the structure with uplift, increased in the low frequency region.

4. Controlled uplift

The increase of horizontal displacement at the top of the structure was due to the footing rotation. It is hypothesized that the footing rotation can be reduced by applying a larger footing weight.

It is necessary to determine how much additional footing weight can be applied on the footing. Using static equilibrium, the moment to resist footing uplift (M_R) and the moment at the footing (M_F) caused by a horizontal acceleration (a) activated at the floor masses are calculated as follows

$$M_F = \sum_{i=0}^{n} m_i \times h_i \times a_i \quad (4)$$

$$M_R = \sum_{i=0}^{n} m_i \times b \times g \quad (5)$$

where b is the half footing width; g is the gravitational acceleration; n is the number of storey; h_i and m_i is respectively the height and the mass of the i^{th} floor; a_i is the floor acceleration before uplift takes place. i=0 represents the footing of the structure.

Base on static moment equilibrium, uplift will take place on one edge of the footing if

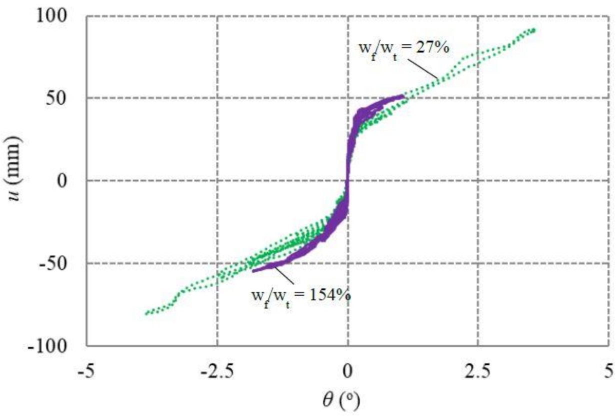

Fig. 15 Reduction of the maximum horizontal displacement and footing rotation due to an additional footing weight

$$M_F = M_R \quad (6)$$

Using the horizontal acceleration at each floor prior to uplift, a 37.6 Nm moment at the footing was calculated. The footing weight (w_f) was 15.7 N and the total storey weight (w_t from the sum of active mass) was 57.8 N. The moment resistance for footing uplift was 18.2 Nm.

To reduce the footing uplift, 7.5 kg mass was applied at the centre of the footing. The footing weight (w_f) was increased to 89.3 N. The footing weight to total storey weight ratio (w_t/w_f) was increased from 27% to 154% (Table 3), resulting in an additional 17.3 Nm moment to resist footing uplift. The sum of the moment to resist uplift was 36.5 Nm. Uplift can thus still be initiated.

Fig. 15 shows the relationship between the displacement at the top of the structure and the rotation at the footing. The additional weight on the footing can reduce the uplift amplitude. When uplift was initiated, the additional footing weight caused less footing rotation. The maximum footing rotations without and with the additional footing weight are 3.9° and 1.8°, respectively. As a result, the maximum lateral displacement at the top of the structure is 54.8 mm. Compared to the maximum horizontal displacement of structure without additional footing weight (92.4 mm, also see Fig. 14), the horizontal displacement of structure without additional footing weight is 69% larger than that of structure with additional footing weight.

Fig. 16 summarizes the maximum horizontal displacement at each level of the structure relative to the ground. For both cases, the horizontal displacement increased almost linearly. This is because the horizontal displacement is dominated by the uplift initiated rigid body motion of the structure. On average, the horizontal displacement at each level from the first floor to the roof of the structure, without additional weight was 22.6 mm, 42.7 mm, 62.3 mm and 80.9 mm, respectively. With an additional weight, the corresponding displacements were only 11.2 mm, 26.1 mm, 37.8 mm and 46.3 mm.

When an additional weight was applied to the footing, the inter-storey drift in the structure increased. Fig. 17(a) shows the maximum inter-storey drift developed in the structure due to all considered excitations. The maximum inter-storey drift, on average is 4.1%, 6.1%, 5.9% and 4.0%

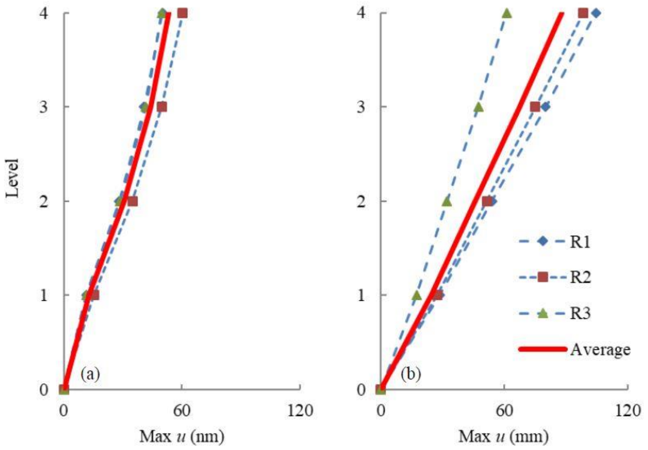

Fig. 16 Horizontal movement of the upliftable structure (a) with, and (b) without additional footing weight due to R3

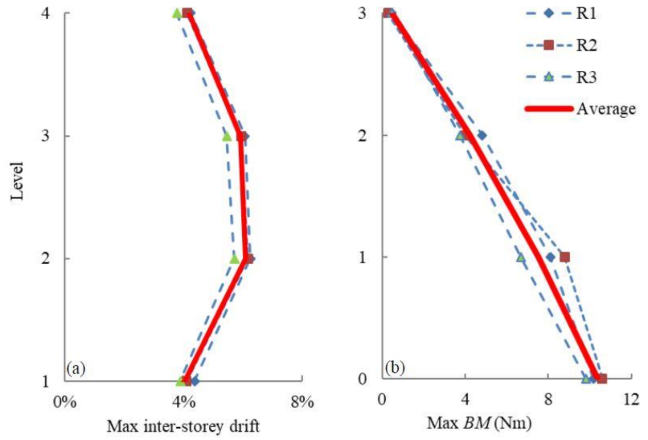

Fig. 17 Maximum (a) inter-storey drift and (b) storey bending moment in the structure with an additional footing weight (w_f/w_t=154%)

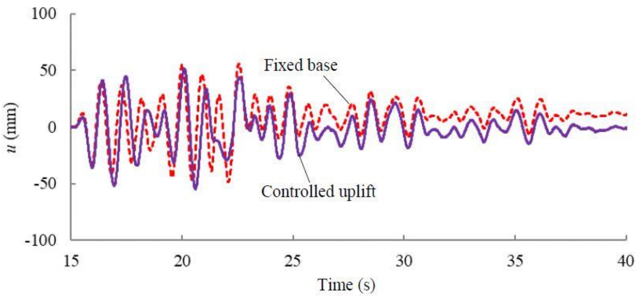

Fig. 18 Horizontal displacement at the top of the nonlinear structure with fixed base and controlled uplift due to R3

for the first floor to the roof level, respectively. Compared to the results in Fig 14(a), the maximum inter-storey drift on average increases by 36%, 22%, 48% and 33% for the first floor to the roof level, respectively. Fig. 17(b) shows the maximum storey bending moment at each level. Applying additional weight on the footing increases the storey bending moment.

Fig. 18 shows that the maximum horizontal displacement at the top of the structure with fixed base was 55.6 mm. In comparison, the maximum horizontal

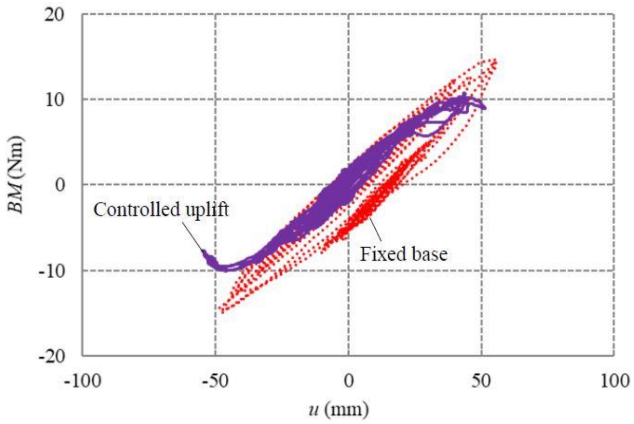

Fig. 19 Avoiding plastic hinge in the structure through controlled uplift due to an additional footing weight

displacement at the top of the structure with an additional weight was 54.8 mm. In this case, uplift even slightly reduces the horizontal displacement of the structure. Thus, the likelihood of pounding against adjacent structures will not increase.

Fig. 19 shows the relationship between the horizontal displacement at the roof of the structure and the storey bending moment at the ground floor. As shown, plastic hinges in the structure with uplift, can still be avoided with the additional footing weight. Considering different excitation on the structure with additional footing weight, no plastic hinge development is evidence. Since uplift reduced the bending moment in the structure, plastic hinge development was avoided. No residual displacement was observed in the structure.

According to Eqs. (4)-(6) an additional 10 kg footing mass, equivalent to a total moment resistance of 41.24 Nm, will eliminate uplift. The footing weight to total storey weight ratio (w_f/w_t) was 195%. In the experiments, however, uplifts took place. The reason is when horizontal displacements developed in the structure, the weight of floor does not act at the centre of the footing. The moment to resist uplift provided by the floor weight should, therefore, be calculated using the actual horizontal distance between the floor mass and the footing edge, rather than half the foundation width (b). Thus, Eq. (5) is modified to Eq. (7).

$$M_R = \sum_{i=0}^{n} m_i \times (b - h_i) \times g \qquad (7)$$

where u_i is the horizontal displacement at the i^{th} floor prior uplift occurs.

Using the acceleration and displacement at each floor level before uplift occurs, the moment to resist uplift M_R and the moment at the footing M_F caused by horizontal accelerations are calculated to be 39.75 Nm and 42.2 Nm, respectively. Thus, uplift can take place. It is confirmed that the estimation of the moment to resist uplift can be more accurate if the response of the structure is considered.

Fig. 20 shows the relationship between the horizontal displacement at the top of the structure and the rotation at the footing. Because of the larger additional footing weight,

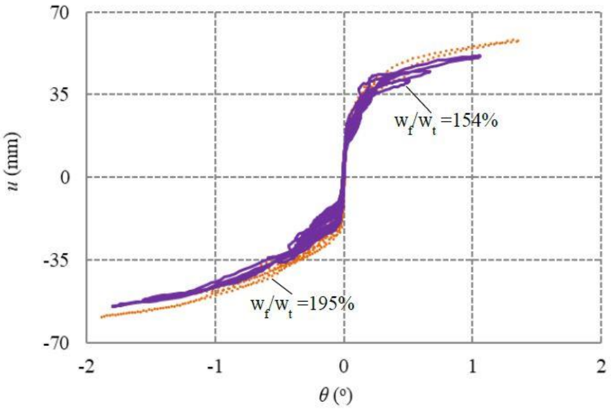

Fig. 20 Consequence of additional footing weight for the top displacement-footing rotation relationship

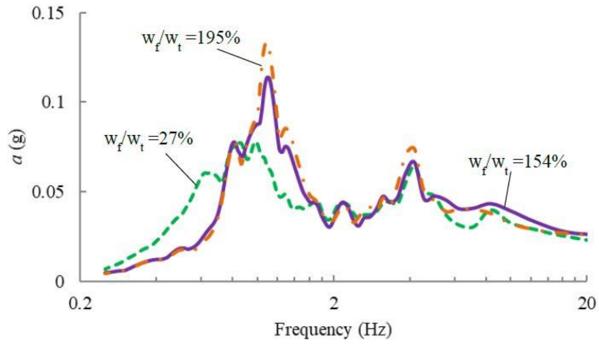

Fig. 21 Effect of controlled uplift due to additional footing weight on the induced vibration to a secondary structure (R3)

a slightly larger horizontal displacement developed in the structure prior to uplift. The maximum horizontal displacement of the structure with the larger footing weight was also greater than that with the smaller weight. This could be attributed to the interaction between the structural response and the footing response. With a larger footing mass, the rotational inertia of the footing increases. Although a greater moment to resist footing uplift was applied, the footing rotation interacted with the structural response. The footing with the larger weight (dotted line) had a larger rotation and caused a greater horizontal displacement of the structure. When w_f/w_t=195%, the maximum horizontal displacement and footing rotation was 59.1 mm and 1.9 ^{o}, respectively.

With an additional footing weight, the response period of the structure with uplift is also reduced (see solid lines in Figs. 14 and 18), and this in turn affects the induced vibrations on the secondary structure. Fig. 21 compares the response spectrum of induced accelerations at the top of the structure with different footing weights. Overall, the spectrum accelerations of structure without additional footing mass were larger in the low frequency range (lower than 0.72 Hz). However, the additional footing mass caused a larger footing rotational inertia. The elastic deformation of the structure interacts with the footing rotation during uplift. This interaction increases the higher modes contribution to the structural response. At the frequency around 1.1 Hz and 4.1 Hz, the spectrum acceleration of the structure increase with the footing weight.

However, a greater footing weight might not always cause a larger induced vibration in the high frequency range. In the frequency range greater than 6 Hz, the spectrum acceleration of the structure with w_f/w_t=154% is the highest. It is concluded that footing weight and higher modes of vibration associated with the upliftable structure have a large influence on the induced vibration of the secondary structure.

5. Conclusions

This work investigates the feasibility of achieving low damage seismic design of a structure through allowing structural uplift. A multi-storey structural model is used. The model structure properly simulates the plastic hinge development in the prototype. Shake table tests on the structure with fixed base and allowable uplift considering different footing masses were carried out using three earthquake records. The plastic hinge development, drift performance, and bending moment distribution in the structure were studied. The impacts of induced vibrations on potential secondary structures are also investigated.

This investigation reveals that:

• Plastic hinges in the structure can reduce the effect of induced vibration on secondary structures. When uplift is allowed, the induced vibrations can be further reduced especially in high frequency range.

• To take advantage of uplift effect and at the same time to avoid possible large uplift induced horizontal displacement, the uplift can be controlled by considering additional mass at the footing.

• With additional footing mass, the inter-storey drift and storey bending moments may increase. But the development of plastic hinges in the structure can still be avoided.

• With additional footing weight, the contribution of higher mode to the response of upliftable structure may increase.

Acknowledgments

The authors would like to thank the Ministry of Business, Innovation and Employment for the support of this research through the Natural Hazards Research Platform under the Award 3703249.

References

Beck, J.L. and Skinner, R.I. (1973), “The seismic response of a reinforced concrete bridge pier designed to step”, *Earthq. Eng. Struct. Dyn.*, **2**, 343-358.

Buckingham, E. (1914), “Illustrations of the use of dimensional analysis. On physically similar systems”, *Phys. Rev.*, **4**(4), 354-377.

Chen, Y.H., Liao, W.H., Lee, C.L. and Wang, Y.P. (2006), “Seismic isolation of viaduct piers by means of a rocking mechanism”,

Earthq. Eng. Struct. Dyn., **35**, 713-736
Chopra, A.K. and Yim, S.C.S. (1985), "Simplified earthquake analysis of structure with foundation uplift", *ASCE J. Struct. Eng.*, **111**(4), 906-930.
Chouw, N and Hao, H. (2012), "Pounding damage to buildings and bridges in the 22 February Christchurch earthquake", *Int. J. Protec. Struct.*, **3**(2), 123-139.
Dowdell, D.J. and Hamersley, B.A. (2000), "Lions' gate bridge north approach-seismic retrofit", *Behaviour of Steel Structures in Seismic Areas, Proc. of STESSA*, 319-326.
Fardis, M.N., Schetakis, A. and Strepelias, E. (2013), "RC buildings retrofitted by converting frame bays into RC walls", *Bull. Earthq. Eng.*, **11**(5), 1541-1561.
Federal Emergency Management Agency (2000), FEMA 356. Prestandard and Commentary for the Seismic Rehabilitation of Buildings, Washington, D.C..
Housner, G.W. (1963), "The behavior of inverted pendulum structures during earthquakes", *Bull. Seismol. Soc. Am.*, **53**(2), 403-417.
Ichinose, T. (1986), "Rocking motion of slender elastic body on rigid floor", *Bull. NZ Nat. Soc. Earthq. Eng.*, **19**(1), 18-27.
Kafle, B., Lim, N., Lumantarna, E., Gad, E.F. and Wilson, J. (2015), "Overturning of precast RC columns in conditions of moderate ground shaking", *Earthq. Struct*., **8**(1), 1-18.
Kelly, T.E. (2009), "Tentative seismic design guidelines for rocking structures", *Bull. NZ Nat. Soc. Earthq. Eng.*, **42**(4), 239-274.
Loo, W., Quenneville, P. and Chouw, N. (2015), "A low damage and ductile rocking timber wall with passive energy dissipation devices", *Earthq. Struct*., **9**(1), 127-143.
NZS1170.5 (2004), Structural Design Actions Part 5: Earthquake Action, Standard New Zealand.
Oyarzo-vera, C., Mcverry, G. and Ingham, J. (2012), "Seismic zonation and default suite of ground-motion records for time-history analysis in the North Island of New Zealand", *Earthq. Spectra*, **28**(22), 667-688.
PEER. PEER Next Generation of Ground-Motion Attenuation Models Data Base, http://peer.berkeley.edu/nga.
Psycharis, I.N. (1991), "Effect of base uplift on dynamic response of SDOF structure", *ASCE J. Struct. Eng.*, **117**(3), 733-754.
Qin, X. and Chouw, N. (2017), "Shake table study on the effect of Mainshock-Aftershock sequences on structures with SFSI", *Shock Vib.*, Article ID 9850915, 12.
Sharpe, R.D. and Skinner, R.I. (1983), "The seismic design of an industrial chimney with rocking base", *Bull. NZ Nat. Soc. Earthq. Eng.*, **16**(2), 98-106.

CC